Assessing Strain Fields in Unbalanced Unidirectional Non-Crimp Fabrics

Eleazar A. Trejo [1], Mehdi Ghazimoradi [1], Clifford Butcher [1], John Montesano [1] *

[1] Department of Mechanical & Mechatronics Engineering, University of Waterloo, 200 University Ave. West, Waterloo N2L 3G1, Canada

* Corresponding Author: John Montesano, Director - Composites Research Group (john.montesano@uwaterloo.ca)

Abstract

Automation of fabric preforming for resin transfer moulded composite parts motivates the need to characterize the response of dry fabric, which is required for the development of simulation models to predict potential draping defects. In this study, the in-plane tensile-shear response of a heavy-tow unidirectional non-crimp fabric (UD-NCF) subjected to bias tensile loading was investigated. Challenges associated with fabric surface texturization and associated strain measurement through digital image correlation was addressed by using a mixture of oil-based paint and mineral spirits to create a suitable speckle pattern. Custom clamps were also designed to prevent the test specimen from damaging or sliding from the grips. Strain maps revealed that the off-axis extension tests induced combined shear, tensile and compressive strains in the fabric test specimens. The fabric deformation response and proposed methods are relevant aspects for characterizing unbalanced UD-NCFs and calibrating corresponding draping simulation models.

Keywords: A. Carbon fibers; A. Fabrics/Textiles; D. Mechanical testing; E. Preforming.

1. Introduction

Out-of-autoclave processing techniques for fiber-reinforced plastic (FRP) composite parts, such as resin transfer molding (RTM) and liquid compression molding (LCM), utilize dry fabric reinforcements and a liquid resin. In comparison to widely used processes employing prepreg materials, RTM and LCM are cost-effective alternatives to fabricate FRP composite parts [1,2]. A highly promising process for high volume production part fabrication is high pressure resin transfer molding (HP-RTM) [3]. High production rates and robust process controls can be achieved by utilizing automated fabric preforming, thus enabling complex shaped components to be efficiently processed. Preforming of the fabric layers prior to resin injection is a key step of the HP-RTM processes, which involves draping within the mold itself or more commonly using a separate draping tool [4]. One of the challenges with automated draping is that defects such as wrinkling and large shear deformations can be introduced into the dry fabric. Therefore, simulation of the draping process can be utilized to predict these defects and optimize the fabrication process [5–7]. To this end, characterization of the corresponding fabric response becomes essential to calibrate a draping simulation model.

Technical fabrics may exhibit several deformation modes when formed, including in-plane shear, compression and tension, as well as bending and out-of-plane compression. These deformation modes are dependent on many factors, where the specific fabric architecture, tow/yarn size and part geometry are among the most influential. Therefore, modelling fabric draping induced deformation may require the use of a combination of several superimposed deformation modes. With regards to the constitutive characterization of fabrics, many studies have highlighted the importance of in-plane shear deformation for calibration of draping simulation models [8–13].

Non-crimp fabrics (NCF) have gained popularity as potential reinforcement materials for lightweight composites in various structural applications due in part to the reduced cost when compared to more conventional woven or braided textiles [14]. In addition, composite parts with NCF reinforcements can exhibit superior in-plane tensile properties when compared to those with woven or braided reinforcements, given that the tows are non-crimped [15,16]. By using NCFs with an RTM or HP-RTM process, cost-effective parts can be fabricated [17,18]. There are three major types of NCF depending on the number of fiber directions: unidirectional non-crimp fabrics (UD-NCF), biaxial NCF (commonly known as NCF) and triaxial NCF, composed of one, two and three fiber directions respectively [19]. Recently, due to their flexibility and lightweight design potential UD-NCFs with different stitching and tow architectures have received considerable attention for structural applications in different industries including the automotive sector [5,10,20–22]. However, NCFs have not been widely utilized in the automotive industry to date [23,24]. Since the mechanics of UD-NCFs are governed by their specific internal architecture, it is important to evaluate the factors affecting their mechanical behaviour by considering their in-plane and out-of-plane deformation modes.

Similar to woven fabrics, shear deformation is a critical deformation mode in UD-NCF forming. Many studies have focused on the shear behaviour of woven fabrics [12,25–29] and braided fabrics [30,31], while only a few have been reported in the literature on the shear characterization of UD-NCFs [9,10,32]. Although no standard method exists to characterize the shear response of fabric reinforcement, two different approaches are typically used. The first test is a bias extension test where the fabric principal direction is at 45° with regard to the applied tensile load, while the second involves testing using a dedicated shear fixture called a 'picture frame' [11,12,23,25,26]. From a practical perspective the bias extension test is relatively simple to perform without the need of a complex fixture, while the same fixture can also be used to perform transverse tension tests which are required for characterizing UD-NCFs.

Capturing the local shear strains during a bias extension test is a critical aspect of characterizing the shear response of fabrics and assessing their underlying deformation mechanisms. For a UD-NCF subjected to a bias extension load, the test specimen would inevitably undergo combined shear, and transverse normal strain [10,16]. Thus, it is necessary to isolate the measurement of these strain components during the bias extension test. Due to practical limitations of using strain gauges or other surface bonded sensors, non-contact strain measurement methods must be used for fabric characterization testing. Non-contact methods such as interferometric and white-light-optical methods have been increasingly used in the field of experimental solid mechanics [33]. However, these and other methods have their limitations for fabric characterization testing as they require a continuous surface with low reflectivity and are only able to scan small surface areas. One non-contact approach that may be suitable for mapping shear strains in fabrics, in particular for UD-NCFs, is the well-established digital image correlation (DIC) technique [34]. Nevertheless, DIC may also be challenging to implement on UD-NCFs since shearing of the fabric during a test may be hindered by the surface texturization treatment required to perform DIC analysis.

An additional challenge with testing UD-NCFs is the tendency of the fabric to slide out of the clamps or fracture within the clamps when subjected to tensile off-axis or transverse loading as reported in [10]. Contrary to well-studied bi-axial fabrics, understanding of the clamping-fabric interface interaction remains elusive for UD-NCF, which would be otherwise critical for obtaining accurate and consistent fabric characterization data. Thus, a need exists to investigate suitable methods for testing mechanical behaviour of UD-NCFs.

The primary objective of this study was to investigate the local shear strain response and corresponding interaction of local deformation modes using DIC strain measurements for a heavy-tow UD-NCF subjected to bias tensile loading. To implement DIC strain measurement on the fabric three different paint techniques were evaluated with respect to the accuracy of the measured shear strain. Additionally, an appropriate test methodology to accurately characterize the mechanical properties of the fabric was developed. A clamp design was proposed to prevent common issues such as breaking and sliding of fabric components during transverse extension tests, which represents a challenging test condition for this assessment. The developed test protocol and the constitutive response of the fabric are important for accurately characterizing UD-NCFs to support the development of draping simulation models.

2. Extension tests for UD-NCF

In previous studies the uniaxial bias extension test has been used extensively for the characterization of the trellis mechanism of biaxial fabrics, including biaxial NCF, woven, braided, and knitted [6,16,28,35]. The test set-up consists of a rectangular specimen clamped on the vertical ends with the warp and weft yarns oriented along the ±45° directions, as seen in Fig. 1a. Woven fabrics are known to develop three distinct shear strain regions during 45° bias extension tests, the formation of which are subject to the limitation of the specimen length (l_0) being at least twice as long as the initial width (w_0) [8]. In general, deformation regions A, B and C (see Fig. 1a) correspond to full, half and no shear deformation. Conversely, for UD-NCFs these three distinct regions are not generated during the 45° bias extension test [16,19]. UD-NCFs subjected to off-axis tensile loading deform with superimposition of shear, tensile and compressive deformation modes [10]. These modes are not reflected in the hypotheses behind the pure shear theory used to describe deformations in the bias-extension test, which result in the generation of shear regions A, B and C [16,36]. Due to this significant difference the test is referred to as the 45° off-axis extension test in this paper (see Fig. 1b). Conversely, if the off-axis angle is increased to 90°, the UD-NCF is subjected to a load along the direction transverse to the fiber tows; this case is referred to as a transverse extension test.

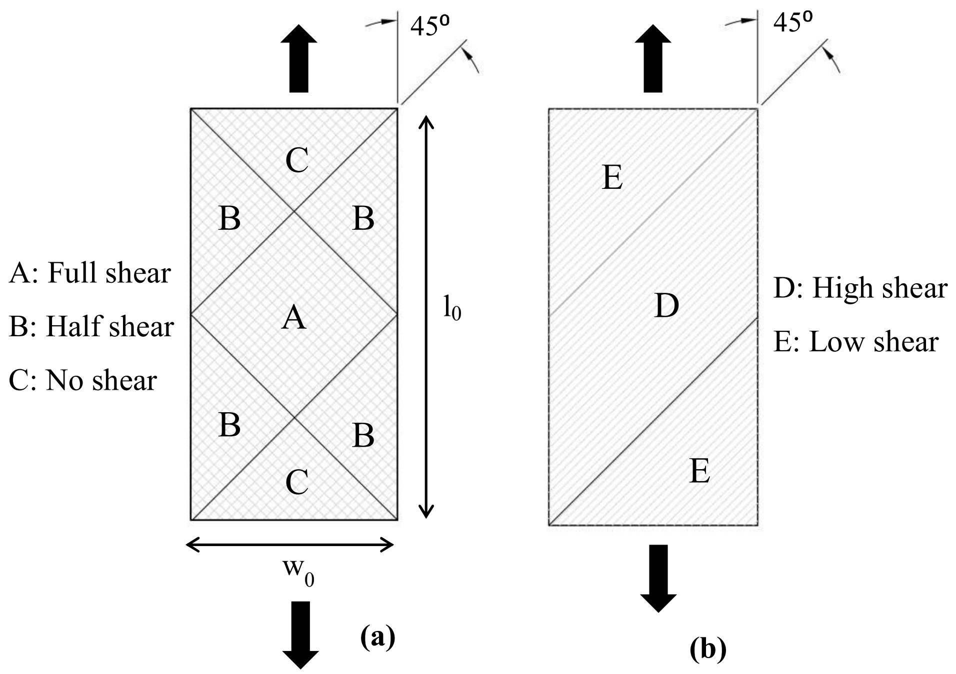

Fig. 1. Schematic of (a) the bias extension test for woven fabrics, and (b) 45° off-axis test for unidirectional non-crimp fabrics.

3. Digital image correlation for UD-NCF

In this study, two-dimensional digital image correlation (2D-DIC), VIC-2D from Correlated Solutions Inc. was utilized. A single camera perpendicular to the surface of the specimen was used to capture deformations throughout the full specimen surface area. It should be noted that for all the tests performed in this study visual inspection confirmed that no out-of-plane deformations were generated and that strains remained in a single plane, enabling use of 2D DIC.

The accuracy of DIC strain measurement depends upon the ability of the software to track the relative deformation of a high contrast, random speckle pattern in a region of interest (ROI) [37,38]. The user-defined subset parameter must be large enough to contain a statistically distinctive pattern for correlation. The choice of an appropriate subset size depends upon the image resolution in the ROI and the size of the speckles which depends upon the speckling technique. A relatively coarse speckle pattern will limit the strain resolution defined by the subset size. Thus, the painting technique employed to texturize the fabric surface has a direct impact on the resulting quality of the DIC analysis and results [38]. Also, VIC-2D software can perform the DIC analysis using either the first image as the reference image or by using an "incremental option" where the reference image is continuously updated between sequential images. The incremental correlation option was used in all DIC analysis performed in this study.

Dry textiles, such as UD-NCF, are challenging materials to study using DIC due to several reasons. First, UD-NCFs may be susceptible to large shear deformations, complicating deformation tracking. Second, the DIC algorithm approximates the heterogeneous surface of the fabric as a continuum. This approximation may introduce uncertainties caused by surface shifting. For example, a particular fiber filament initially on the surface of the fabric may relocate under the fabric surface during deformation, disappearing from the DIC image. The combination of these factors can lead to pattern breakdown and loss of correlation for fabrics during DIC analysis [39]. Therefore, it is critical to generate a high-quality speckle pattern that produces images with high contrast and feature definition in the grey scale [37].

In this study, DIC analysis was performed on the complete extension test specimen area to compute Green-Lagrange strain maps. A 50 × 50 mm^2 (200 × 200 $pixel^2$) ROI was specified in the middle of the specimen to record average shear strain magnitudes. For all strain computations, a subset size of 55 × 55 $pixel^2$, a step size of 5 pixels, a decay filter size 17, and a typical resolution of 0.2646 mm/pixel were used. Also, a Gaussian weights method option was used for strain calculation since it provides the best balance of spatial and displacement resolution [37]. The following section presents a brief description of the fabric material and the overall test methodology used in the study.

4. Materials and test methodology

The UD-NCF assessed in this study was PX35 UD300 manufactured by Zoltek Corp. (see Fig. 2). This fabric is composed of 5 mm wide heavy tows, each containing 50K carbon fiber (CF) filaments. The tows are all aligned along the warp direction and stitched together with a light polyester thread (76 dtex) using a tricot stitching pattern along the CF tow direction. To facilitate CF tow stitching and provide integrity to the fabric, glass fiber (GF) yarns (34 dtex) oriented perpendicular to the CF tows were placed approximately 3.5 mm apart on one side of the CF tows (see Fig. 2a). On the opposite or stitching pattern side the fabric has a light application of a powder binder resin that cures and stabilizes the fabric preform during high temperature forming. The total fabric areal density is 333 g/m^2, of which the CF tows account for 92.8%.

All tested specimens were cut from a roll of the UD-NCF material with an aspect ratio of 2 and dimensions of 160 mm wide by 320 mm long (see Fig. 2b). For the bias extension test specimens the CFs and the stitching threads were oriented at 45° from the specimen longitudinal axis and load direction, while for the transverse extension test specimen the CFs and stitching were oriented perpendicular to the loading direction. The specimen size and aspect ratio was chosen to match that used in previous studies where fabrics were characterized using bias-extension tests [10,35]. Fabric architecture details can be seen in Fig. 2c. All tests were conducted at room temperature on an MTS FlexTest SE servo-hydraulic test frame fitted with an Omega 2.2 kN load cell at a constant displacement rate of 1 mm/s. Images for DIC analysis were captured at 3 frames per second using a Nikon D3200 camera fitted with a Nikon DX Zoom NIKKOR 28-55 MM lens.

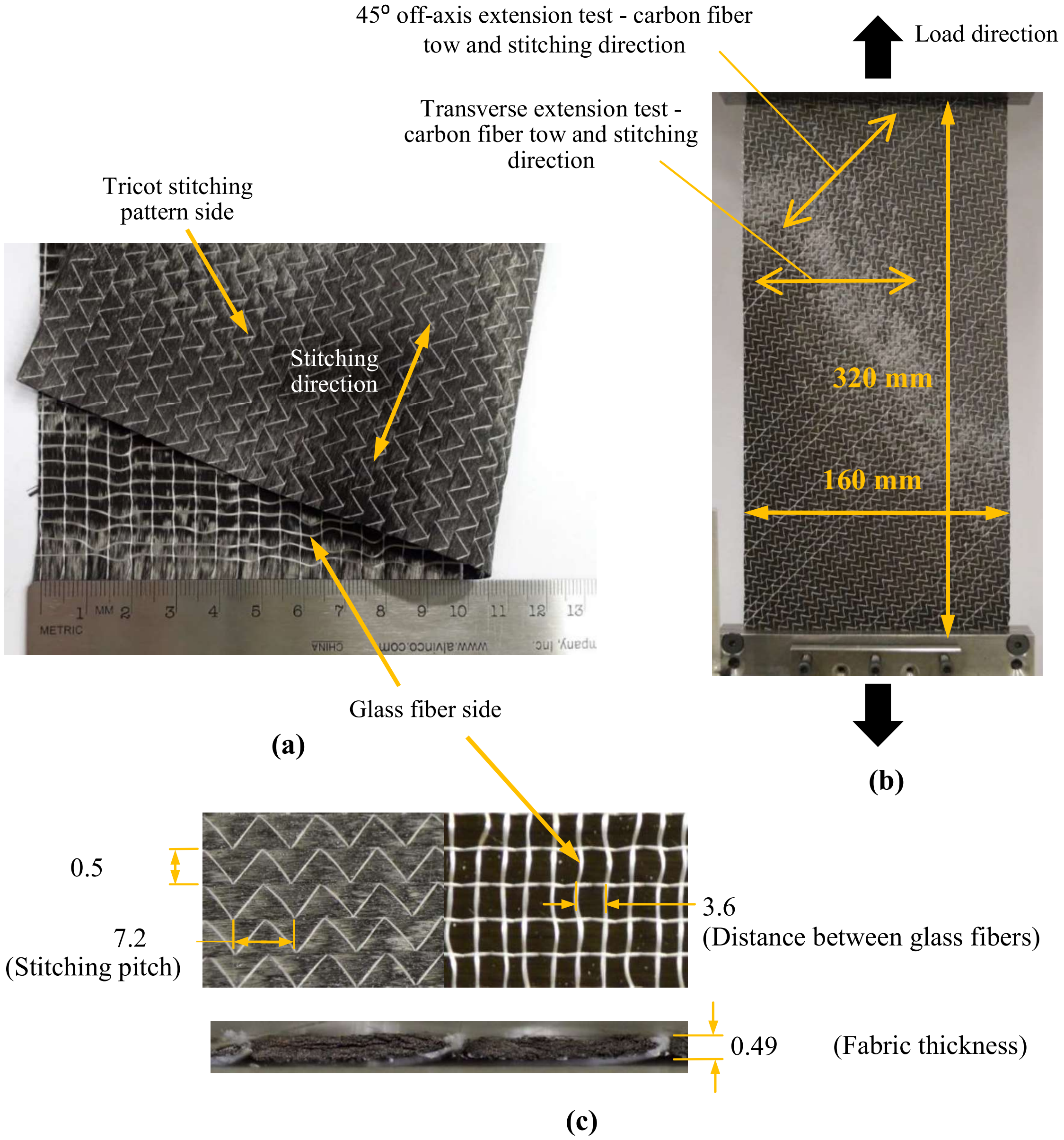

Fig. 2. (a) Investigated UD-NCF, (b) 45° off-axis and transverse extension test specimen configuration, and (c) UD-NCF architecture details.

4.1 Surface texturization techniques

Three different types of paints were tested on the fabric with the aim of creating a surface pattern that could be effectively captured and processed by the DIC software; spray paint, latex paint and oil paint. When using DIC for deformation tracking on composites, it is a standard practice [34,40] to apply a base layer of white spray paint and black markings or speckles on top of it. In this study, this standard technique is referred to as 'spray paint' (see Fig. 3a) and was the first one to be tested.

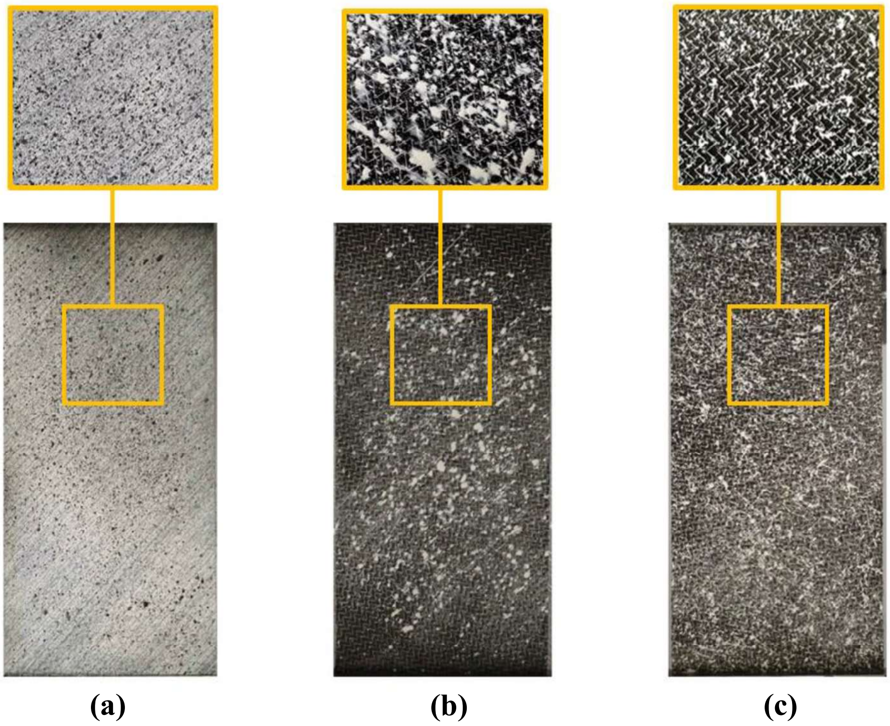

Fig. 3. 45° off-axis extension specimens texturized with (a) spray paint, (b) latex paint, and (c) oil paint.

A second painting technique was implemented using white latex paint to create markings directly on the fabric surface which has a dark contrast. The white markings were generated using a hard bristle brush to disperse the paint. One advantage of using a latex-based paint is that water can be used as a thinning agent to adjust the viscosity of the paint as required. Additionally, latex-based paints produce fewer toxic fumes and dry faster than oil-based paints. Fig. 3b shows the fabric sample that resulted from the application of latex-based paint. The third painting method tested used the same technique for paint application as the latex-paint specimen but with oil-based paint instead. Since oil paints tend to have high viscosity, the viscosity was adjusted using a thinning agent such that the most effective consistency was achieved. During the specimen surface texturization process the objective was to create markings that were small enough to reduce their influence on the mechanical properties of the fabric but large enough to prevent absorption by the fabric and to ensure surface tracking by the DIC system. The best oil-paint result is shown in Fig. 3c and was produced by mixing 1 quart of oil-based paint (946 ml) with 60 ml of mineral spirits thinning agent. This is equivalent to around 6% ml/ml mineral spirit mixture concentration.

4.2 UD-NCF clamping

The off-axis and transverse tensile behavior of UD-NCFs is strongly dependent upon the boundary conditions applied to the specimen. Tensile deformation along the transverse direction is particularly sensitive to the applied boundary conditions since the GFs have a tendency to slide out of the clamps. Schirmaier et al. [10] investigated the problem of sliding GFs during unidirectional transverse tensile tests on UD-NCFs, noting that variations in the boundary conditions significantly impacted the transverse behavior of the fabric. It was observed that the reported material stiffness increased by a factor of ten when the GFs were fully fixed compared with sliding GFs. Fracture of the GF within the grips may also occur which was observed in the present study when the fabric was transverse and in the 45° off-axis extension test specimen as seen in Fig.4. This motivated a redesign of the initial clamps, which featured a sharp bend V-notch as shown in Fig. 5a. In the initial clamping approach, two main features were identified to cause the GFs to break, i) sharp bends and ii) high clamping forces.

A clamping mechanism was proposed to prevent fabric and GF slippage, while maintaining the integrity of the GFs (see Fig. 5b). Each clamp consisted of two steel plates and a PVC hexagonal rod insert as shown in Fig. 5b, with dimensional details as seen in Fig. 5c. During clamp installation the fabric was wrapped around a PVC rod insert, which was subsequently placed in the pocket formed between the clamps before bolting the two clamp sides together with a torque of approximately 0.212 Nm.

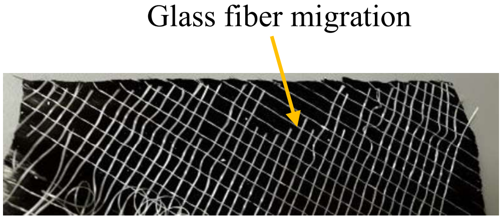

(a)

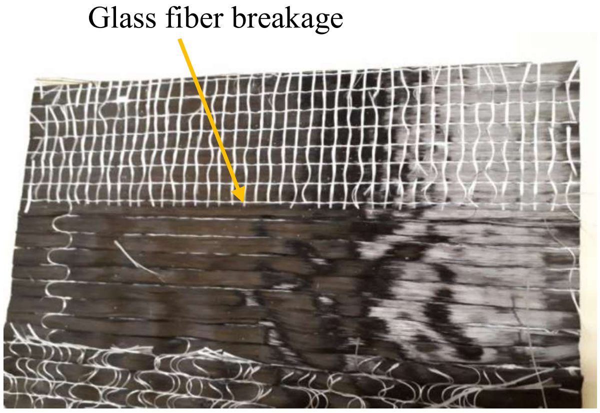

(b)

Fig 4. Clamped region of UD-NCF test specimens: (a) Fiber glass migration caused by low clamping force, and (b) fiber glass breakage caused by high clamping forces and sharp bends in the fixture.

The effectiveness of the clamping was confirmed by the consistency of the load response, as well as by the absence of GF breakage as examined after completing each test. The effect of the clamping redesign in the transverse tensile test was demonstrated through a comparison of the transverse load response with and without GF slippage and breakage as discussed in Section 5.1. The modified clamping was used for both the 45° off-axis and transverse extension tests.

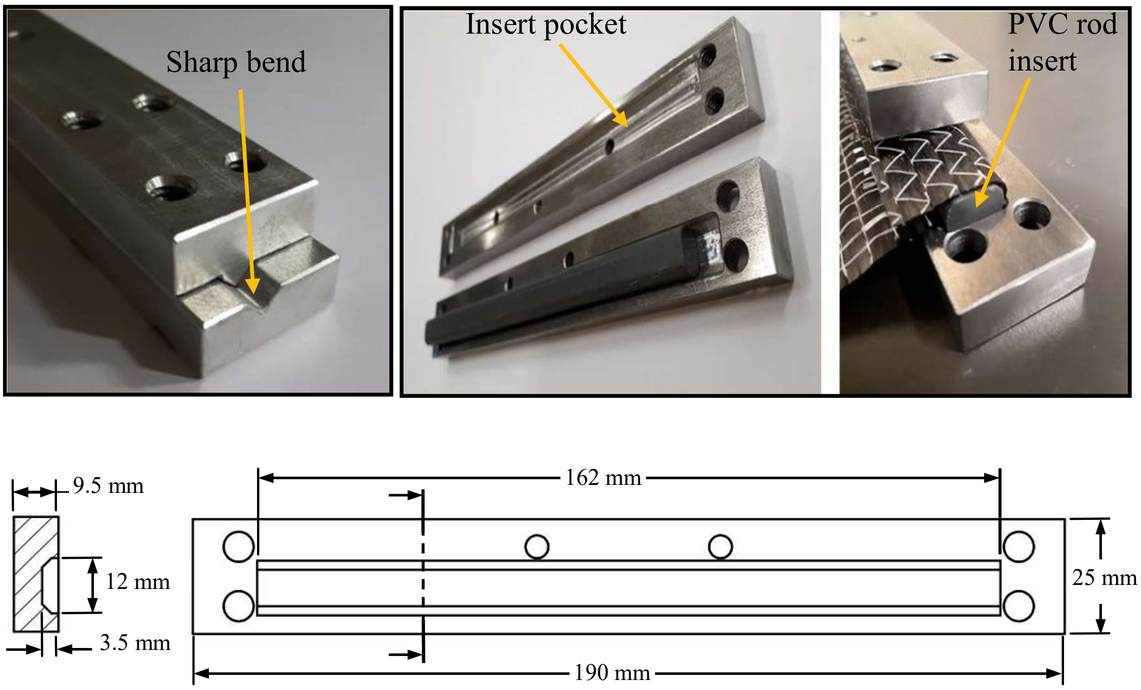

Fig. 5. Extension test clamping fixture for unidirectional non-crimp fabrics. (a) Initial clamp design, (b) redesigned clamping fixture with PVC insert and (c) half-symmetry dimensional details of redesigned clamping fixture.

5. Results and discussion

The results of the 45° off-axis and transverse extension tests are presented in the following subsections. First, the assessment of the susceptibility of the transverse tensile test specimen to clamping conditions is presented. The results of a sensitivity analysis of the macroscopic fabric response for the three different surface texturization methods is presented along with a comparison of DIC-based contour plots of Green-Lagrange shear strain. Finally, a comparison of the overall deformation of a specimen treated with oil paint with that of the bare fabric is shown.

5.1 Fabric clamping under transverse extension

Based on force response behavior and post-test visual examination, as illustrated in Fig. 4, three critical parameters were found to affect the integrity of the fabric inside the clamps: clamping force, contact surface area, and fabric maximum bending curvature. In this context, the fabric maximum bending curvature corresponds to the smallest bending radius that the fabric is subjected to when placed inside the clamping fixture. In agreement with the results reported by Schirmaier [10] on characterization of a similar UD-NCF, the GFs fractured due to the sharp bend produce by the notch-like feature (see Fig. 4a) during the transverse extension tests, while a small clamping area and high clamping forces was also deemed to contribute. To eliminate these features and prevent breakage of the GFs, as previously indicated the clamp was redesigned without sharp bends, the fabric contact area was enlarged, and the torque applied to the clamping bolts was limited to 0.212 Nm (see Fig. 5b).

Figure 6 includes a comparison of the tensile load response for the transverse extension test with fully constrained fabric (i.e., modified clamp design), as well as when GF slippage and GF breakage were observed (i.e., initial clamp design) using the specimen dimensions shown in Fig. 2. The load response behavior when the fabric was fully constrained, with no fabric damage or GF slipping in the clamps, was characterized by an initial low resistance to deformation resulting from straightening of the initially slack GFs. This was followed by a gradual increase in the response up to a linear region where the GF were fully extended and under tensile loading, reaching a peak force of approximately 570 N (see Fig. 6a). After the peak force was attained sequential GF failure was observed within the gauge section of the test specimen, eventually resulting in total loss of specimen stiffness. On the other hand, it is observed that when the GF fractured at the clamps there was little resistance to deformation and the peak load reduced more than 30 times the peak response of the fabric with no damage or slipping. Similarly, when the GFs did not fracture and instead slipped inside the clamp a sudden drop in load was observed in the linear region at a peak force of 280 N which marked the onset of GF slippage. As seen in Fig. 6a, the response curve representing GF slippage initially coincides with the response curve of the fully constrained specimen. The transverse tensile response and corresponding peak load of the fully constrained test specimen obtained using the designed clamps are clear indications of improvements, as demonstrated by the repeated test results shown in Fig. 6b. Note, the variations in the results shown are due to the variability in the sequential failure events of the GFs. Thus, this clamping method was used for all subsequent tests.

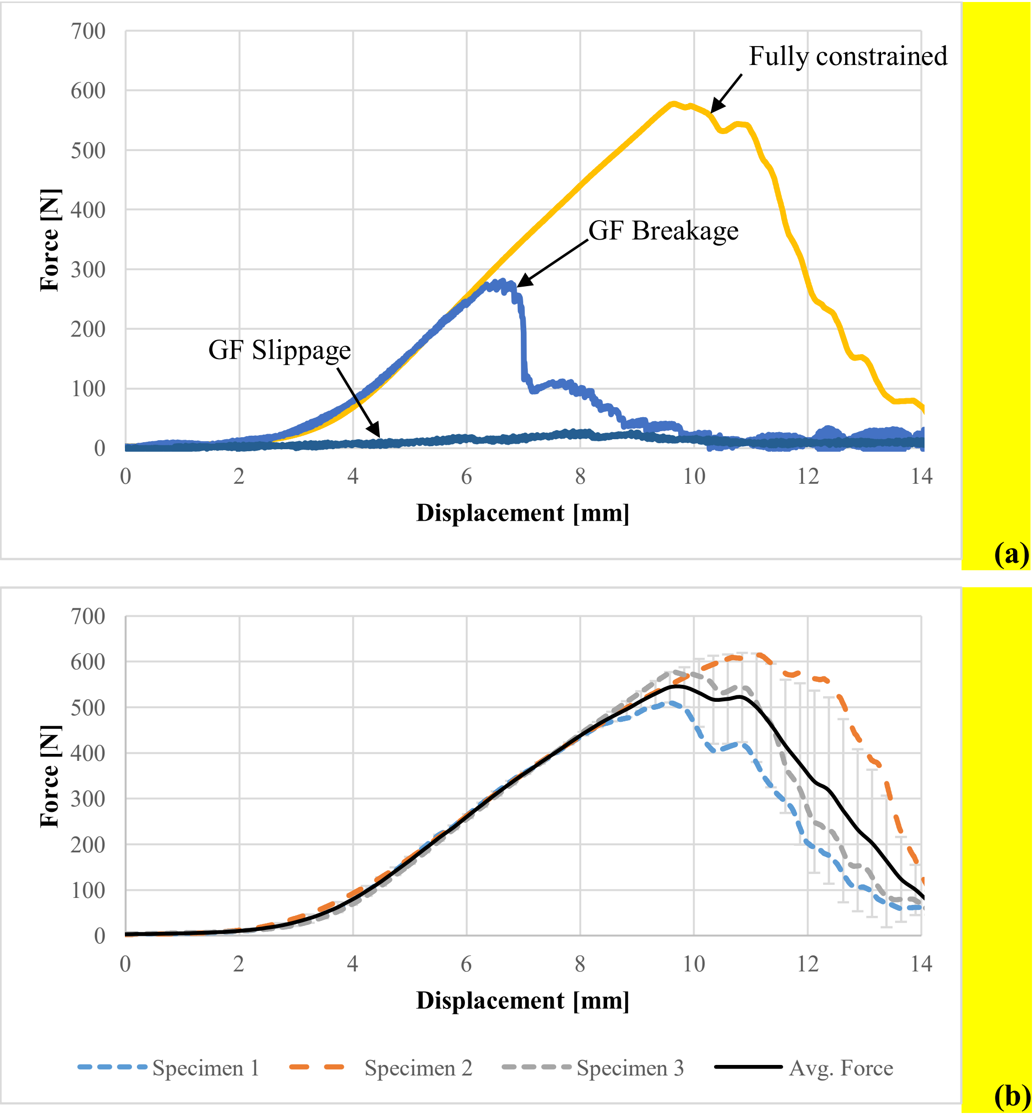

Fig. 6. (a) Comparison of the force responses of the UD-NCF under transverse extension loading with three different clamping scenarios: original clamp with glass fiber breakage due to high clamping pressure, original clamp with glass fiber slippage, and proposed clamp with fully constrained glass fibers. (b) Force versus applied displacement for transverse extension tests with fully constrained clamping.

5.2 Applied load response under 45° off-axis extension

During the 45° off-axis extension tests, deformations along the warp and weft fabric directions were hindered by the high stiffness of the CF tows and GF filaments respectively. Hence, the prevalent mode of deformation was shear. Furthermore, large deformations were commonly seen along the vertical edges and within the free-edge area of the test specimens (see Fig. 7) due to local stitching discontinuities. In the free-edge area, the CF tows were unclamped at both ends, thus load transmission from the clamps into this region relied on the low-stiffness stitching and crimped GFs, concentrating the deformation within this region.

Representative average load-displacement results for the 45° off-axis extension test specimens with three distinct paint techniques, as well as the bare fabric specimen, are shown in Fig. 7 with corresponding data scatter bars. The three texturized test specimens yielded unique load responses, with those using oil paint having the lowest magnitude force response while the spray-painted specimens had the highest. The force response was directly related to the extension of the area affected by paint, which acted as a bonding agent mechanically reinforcing the fabric regions (i.e., tows) it contacted even though only small markings were applied to the fabric. Thus, there is a direct and positive correlation between the surface area covered by the paint and the increase seen in load response.

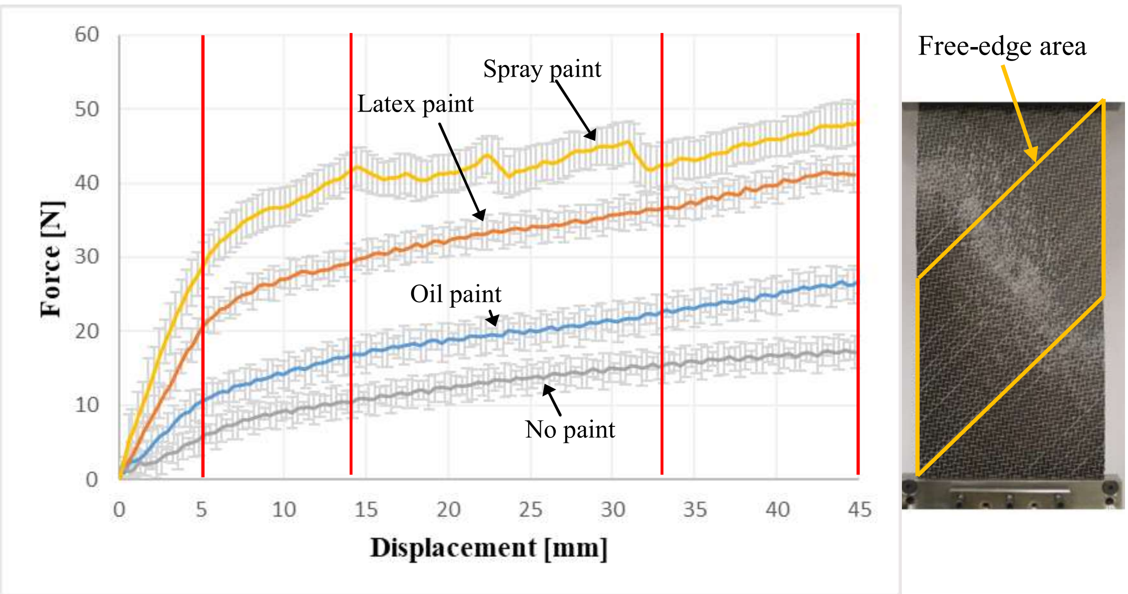

Fig. 7. Force response of 45° off-axis extension test for non-texturized specimen and those texturized with oil paint, latex paint and spray paint.

Three distinct regions were identified along the load-displacement curves for all texturized and bare fabric specimens. An initial linear region extended from 0 to 5 mm of applied displacement, followed by a region of decreasing slope until 14 mm displacement, and a final a quasi-linear region from 15 mm to 45 mm of applied displacement. The displacements shown in Fig. 7 were chosen for subsequent observation and analysis of loading responses and shear strains contour plots.

As observed in Fig. 7, the average load of the oil-paint treated specimen was 6 N higher than the average load of the no-paint specimen after 5 mm of displacement. However, by considering the data scatter bars the load response of the oil-paint treated specimen is within the observed data variability of the no-paint specimen. In fact the variability of the load response is similar in magnitude for both the oil-paint and no-paint specimens and can be associated to imperfections in the fabric including the variation in the dispersion of the binder on the fabric which will influence the shear response. On the other hand, the load responses of the latex- and spray-painted specimens were respectively 4 and 6 times higher than the no-paint specimen, with the spray-painted specimens exhibiting a higher degree of variability. At this low displacement the effect of the paint was already noticeable, with the oil paint surface texturization having the least influence on the load response. At a displacement of 14 mm, the loading curve of the spray-painted specimen showed irregular and sudden load variations resulting from the progressive fracturing of the continuum layer of paint on the surface of the specimen. These large forces suggested that the standard spray paint technique is not suitable for strain measurements of UD-NCFs.

At the same 14 mm displacement, the loading curve of the specimen texturized with latex paint was lower than that of the spray paint specimen. However, the load from this specimen was still 3 times larger than the reference bare fabric specimen. Compared to the spray-paint treated specimen, the loading curve of the latex-paint specimen more closely resembled the reference bare fabric load response. Regarding the oil-paint treated specimen, the average load response was dramatically lower than the spray and latex painted specimens, showing approximately a 6 N increase from the average load response of reference bare fabric loading curve after 14 mm of displacement. Again, by considering the data scatter bands the response of the oil-painted specimens more closely correlated to the no-paint specimens. This significantly lower load response was attributed to the reduced amount of paint and surface area covered by the applied oil-based paint compared to the other two paint methods. The decrease in these two factors was the direct result of higher image definition and contrast produced by oil-paint texturization and the ability to spray small markings while preventing absorption by the fabric.

Regarding variation in the data among the three paint application techniques, the spray paint treated specimen produced the most scatter, whereas the latex and oil-based paint specimens had comparable scatter as the bare fabric specimen. Overall, the load response of the specimen texturized with oil-based paint most closely followed the response of the reference bare fabric specimen (the corresponding fabric deformations will be discussed further in Section 5.4). Also, when compared to latex and spray-painted specimens the surface texturization using oil-based paint produced superior image quality due to enhanced surface adhesion as well as reduced penetration of the paint into the fabric.

5.3 Macroscopic shear strain measurement with DIC

Given the fact that shear deformation is the dominant forming mechanism of textiles, macroscopic measurements of in-plane shear strain were obtained through DIC at the four critical applied displacements previously identified – 5 mm, 14 mm, 33 mm and 45 mm. Complete surface maps of Green-Lagrange strains were calculated using the digital image correlation method discussed in section 3. Additionally, to compare the effect of the different paint methods on the shear strain response of the specimen, representative average strain values were calculated in a 50 x 50 mm^2 ROI located in the center of each specimen, as shown in Fig. 8. Table 1 contains the average shear strain values in global coordinates (ε_{xy}) where the principal axis is aligned with the loading direction, and in material coordinates (ε_{12}) which are aligned with the CF direction (see Fig. 8). The shear strain in the ROI of the no-paint specimen, with respect to the material coordinates, was estimated by image analysis at each of the indicated displacements since DIC could not be used on the bare fabric. These shear strains were computed using the change in angle between the carbon fibers and the stitching, representing the upper limit of the local shear strain since stitching slipping relative to the carbon fiber tows was observed during the test. This intraply slipping was reported in previous studies for the in-plane deformation of NCFs [10,16,36]. It is observed from Table 1 that the local shear strains for the oil-paint specimens correlated well with the bare fabric specimens over the deformation range considered. Therefore, the results of the oil-paint specimen may be a better representation of the average material deformation in the ROI at the center of the specimen.

Table 1. Average shear strain from 50x50 mm^2 region of interest at the center of the specimen. ε_{xy} and ε_{12} are respectively the shear strains with respect to the loading direction and the carbon fiber direction.

Paint Method	Displacement (mm)	Shear Strain, ε_{XY} (mm/mm)	Shear Strain, ε_{12} (mm/mm)
Spray Paint	0	0.000	0.000
	5	0.012	0.002
	14	0.030	0.029
	33	0.050	0.123
	45	0.064	0.194
Latex Paint	0	0.000	0.000
	5	0.008	0.009
	14	0.018	0.071
	33	0.039	0.220
	45	0.047	0.297
Oil Paint	0	0.000	0.000
	5	0.010	0.016
	14	0.022	0.106
	33	0.050	0.264
	45	0.066	0.295
No Paint	0		0.000
	5		0.024
	14		0.105
	33		0.274
	45		0.370

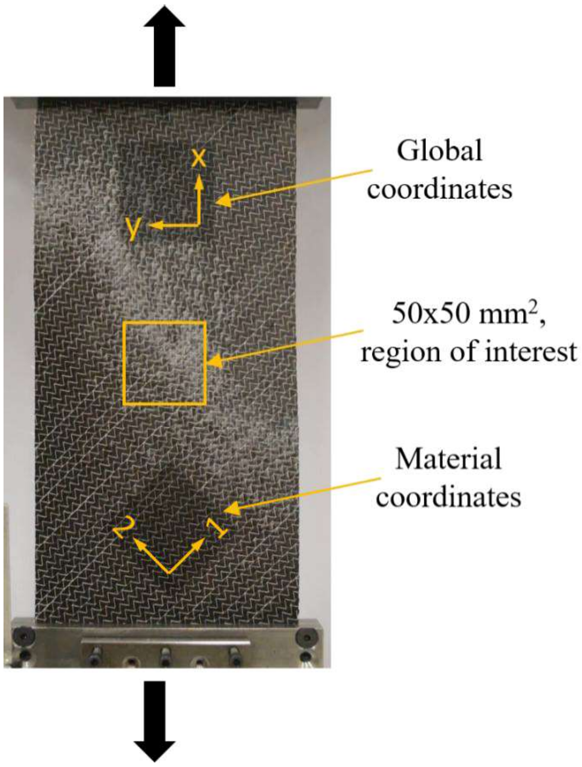

Fig. 8. 45° off-axis extension test global coordinates, material coordinates and region of interest used for strain measurement.

As illustrated in Fig. 9, the oil-paint treated specimen registered the highest shear strain in the material coordinate system, while the spray-painted sample yielded the lowest. The spray paint completely bonded all the surface-exposed components of the fabric, suppressing relative displacements and rotations and effectively preventing full shear deformation. The shear strains seen in the latex-paint treated sample were lower but comparable to the oil-paint treated specimen. The subsequent paragraphs describe the shear strain results represented by contour plots.

As observed in Fig. 10, after 5 mm of crosshead displacement, which is equivalent to 1.56% normal strain along the loading direction, all three specimens exhibited non-uniform shear strain contours and similar peak shear strain readings of approximately 1%. The oil and spray paint texturized specimens show the highest strain developing in the middle section of the free edge area, while shear strain peaks near the free edges are also visible.

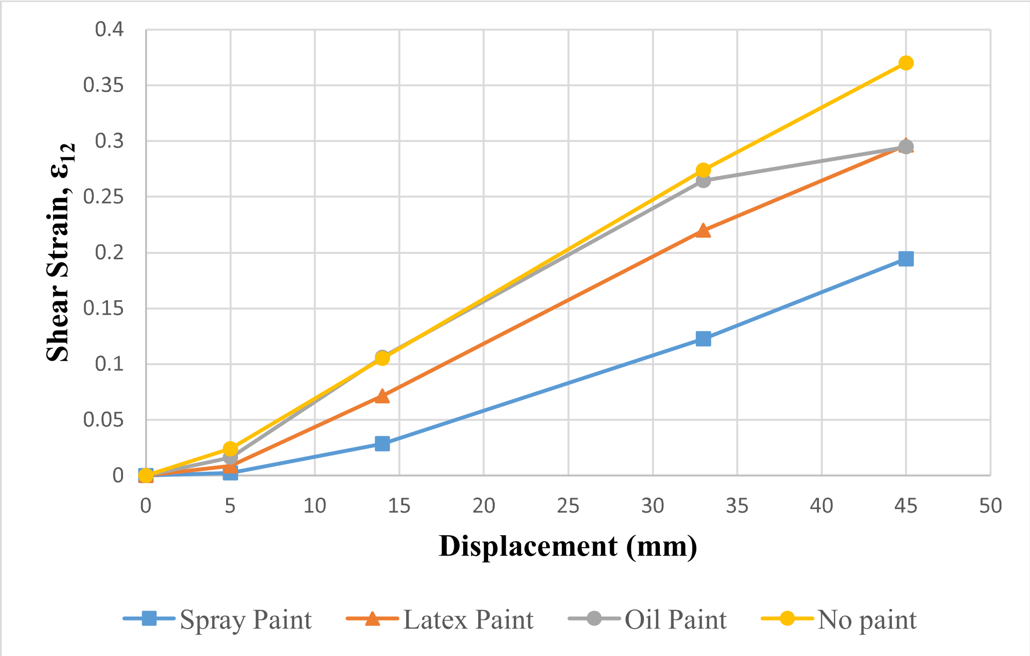

Fig. 9. Comparison of the shear strain in the material direction of the bare fabric specimen with the spray paint, latex paint and oil paint treated specimens.

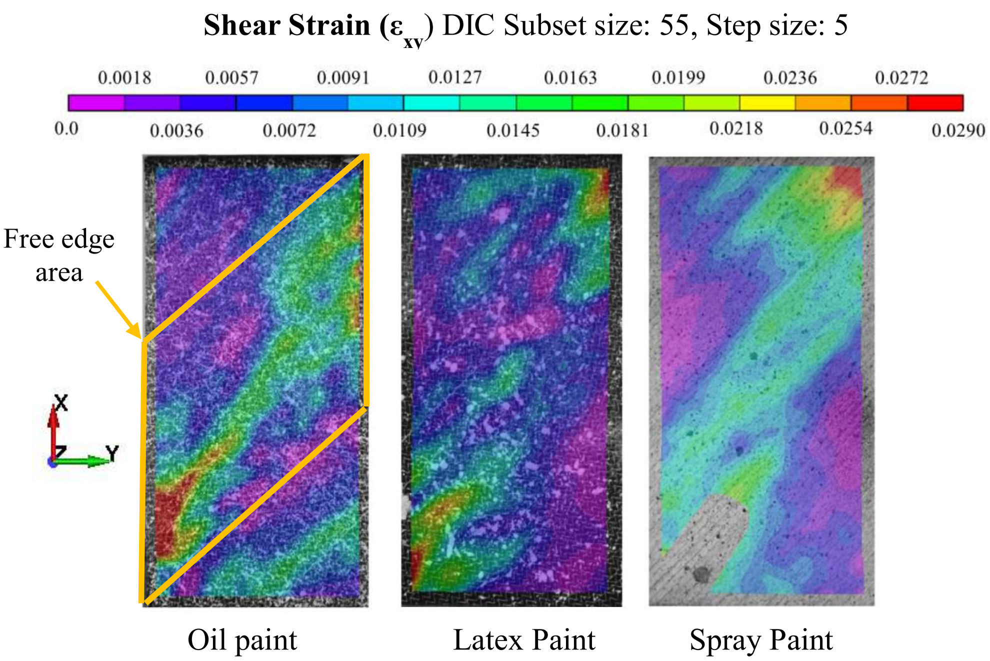

Fig. 10. Shear strain contour plots, after 5 mm vertical displacement, of 45° off-axis extension specimens texturized for DIC using (a) oil paint, (b) latex paint, and (c) spray paint.

At 14 mm displacement or 4.4% normal strain along the loading direction, the oil paint and latex paint specimens showed a similar pattern of strain concentration in the free-edge area as seen in Fig. 11, with the latex paint exhibiting a wider shear band which may be due to the distinct paint systems. On the other hand, the spray paint specimen presented more evenly distributed shear strains and lower magnitude local strains at the center of the specimen.

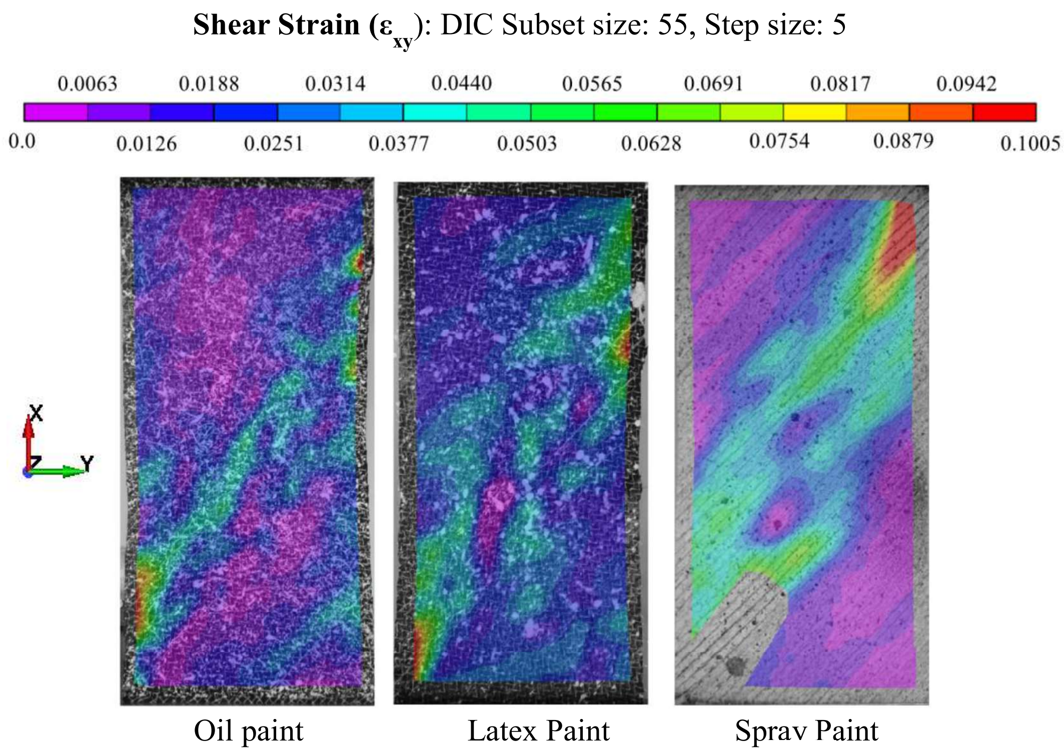

Fig. 11. Shear strain contour plots, after 14 mm vertical displacement, of 45° off-axis extension specimens texturized for DIC using (a) oil paint, (b) latex paint, and (c) spray paint.

At 33 mm displacement or 10.31% normal strain along the loading direction, a notable difference among the specimen strain contours is observed. As seen in Fig. 12, the stitching in the spray-paint treated specimen ruptured close to the clamps. This localized failure consistently appeared in multiple repeated tests at approximately 20 mm of applied displacement, in some instances appearing in the opposite diagonal corner. Note that these ruptures were located close to the clamp in the free-edge area, characterized by unconstrained or unclamped CFs. Also, the spray-paint treated specimen had a tendency to rotate in the clockwise direction, producing high localized stresses at the bottom-left and top-right corners adjacent to the clamps where the ruptures originated. Thus, it was noted that the fabric deformation behavior resulting from the application of spray paint was not reflective of the behavior of bare UD-NCF.

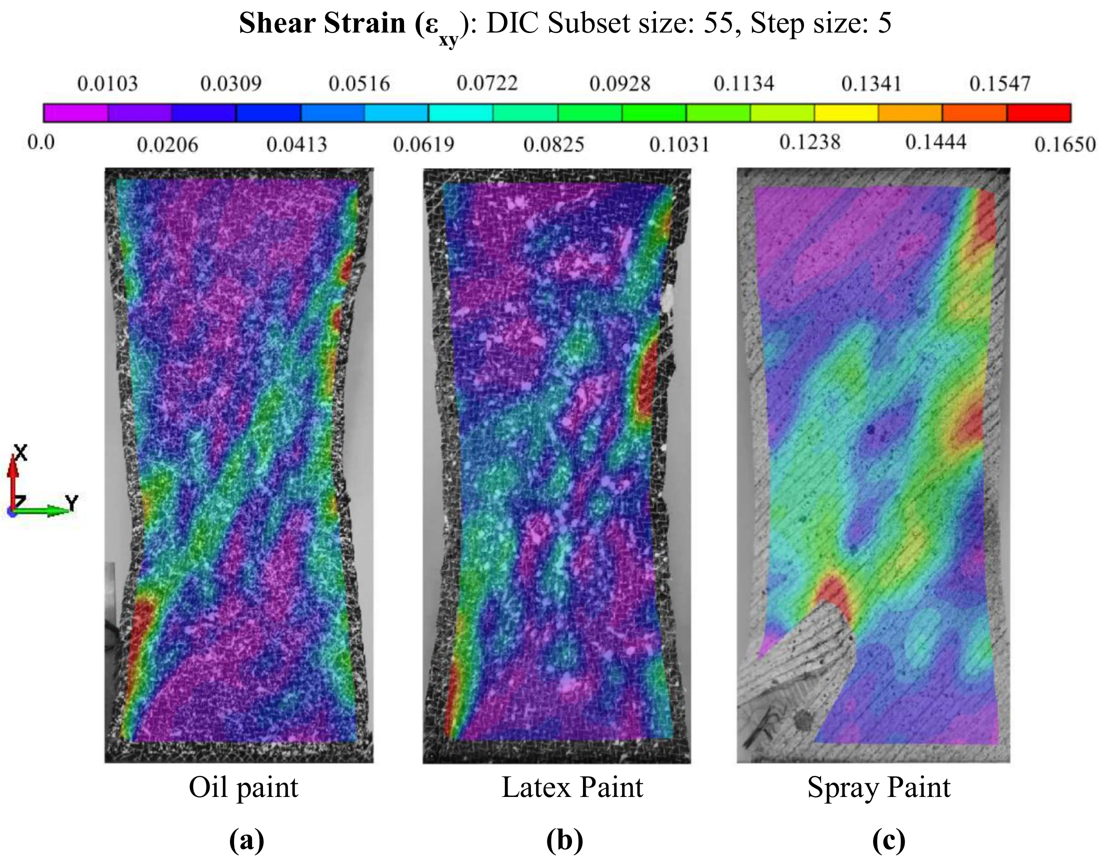

Fig. 12. Shear strain contour plots, after 33 mm vertical displacement, of 45° off-axis extension specimens texturized for DIC using (a) oil paint, (b) latex paint, and (c) spray paint.

With an applied displacement of 45 mm or 14.1% normal strain along the loading direction, it was noticed that oil-paint texturized sample exhibited a shear strain map that best resembled the expected deformation of the bare fabric, as shown in Fig. 13. A region of high strain was seen across the middle diagonal direction, following the direction of the CF tows, and surrounded by areas of lower strain closer to the clamps. Moreover, as would be expected in the bare fabric, the oil-paint specimen also exhibited areas of high strain along the edges. Among the three different paint systems, the specimen texturized with oil paint best emulated the deformation of bare UD-NCF.

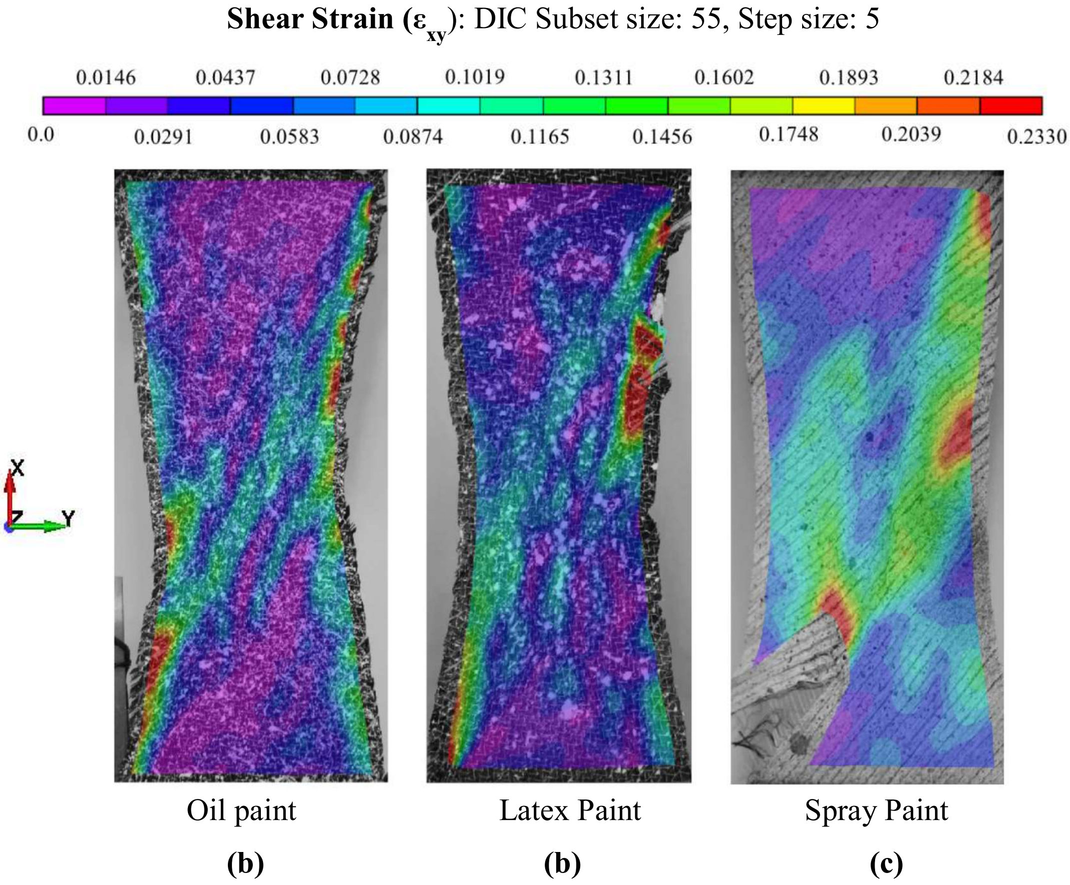

Fig. 13. Shear strain contour plots, after 45 mm vertical displacement, of 45° off-axis extension specimens texturized for DIC using (a) oil paint, (b) latex paint, and (c) spray paint.

A closer look at the normal and shear strains along the material direction within the region of interest revealed important information about the deformation mechanisms of the studied

UD-NCF material. As it can be observed in Fig. 14, the oil and latex-paint texturized specimens followed a similar strain response. The normal longitudinal strain along the CF tow direction, ε_{11}, changes sign from negative at 14 mm displacement to positive at 33 mm displacement. This apparent initial contraction of the CFs is caused by micro-crimping generated by tensioning of the stitching and transverse GFs. Conversely, the normal strain along the transverse CF tow direction, ε_{22}, changes from positive to negative in the same displacement interval. In this case, GF micro-crimping was responsible for low fabric stiffness along the transverse direction, triggering a noticeable initial transverse stretching and shear deformation that dominated the fabric deformation. By the time an applied displacement of 33 mm was attained, the CFs had rotated towards the loading direction. In this position the reduction in area at the center of the specimen due to necking (see Fig. 15) compressed the specimen, inducing negative strains along the transverse direction. It can be appreciated from Fig. 14 that both the application of oil paint and latex paint for fabric texturization produced a similar strain behavior, with the latex-paint treated specimen producing more attenuated deformations. Although the application of oil and latex paint influenced the fabric response to some degree, both of these painting techniques were able to preserve inherent deformation mechanisms of the fabric, with the oil-paint method displaying a higher fidelity to the expected response of the untreated fabric.

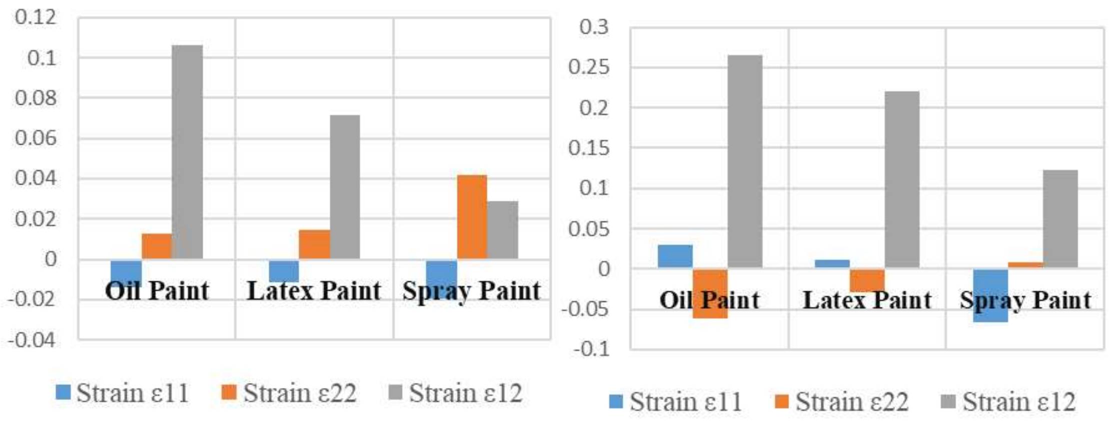

Fig. 14. DIC measured strain values (mm/mm) in the material coordinates, represented by ε_{11}, ε_{22} and ε_{12}, for specimens texturized using oil, latex and spray paint after (a) 14 mm displacement and (b) 33 mm displacement.

5.4 Comparison of oil paint and no-paint specimen overall deformation

As previously mentioned, oil-paint texturization interfered the least with the intrinsic mechanism of deformation of the fabric, minimizing the effect that the paint had on load response and local deformation compared to the other two surface texturization methods. A comparison of the oil-paint texturized specimen and a bare specimen showed that the overall deformation is consistent among the two (see Fig. 15).

There were clear similarities between the two samples. Both samples showed an inward taper, or necking, starting from the clamp towards the center. Also, they both exhibited tow gapping in scattered locations along the vertical edges where the stitching yarns were discontinuous. These edge gaps were expected since deformation concentrated where the stitching was weak producing openings between the CF tows. Additionally, Fig. 15c shows a comparison of the shear strain evolution at the center of the oil-painted and no-paint specimens. There is a strong correlation up to a normal strain of 10%, after which the oil-painted specimen strain measurement diverges with a lower magnitude. This difference after 10% normal strain is believed to be a consequence of using the stitching to approximate the shear strains in the bare fabric, where DIC could not be applied. The shear strain in the bare fabric was approximated using the rotations of the carbon fibers filaments relative to the stitching, which tended to slip relative to the CF filaments as the applied normal deformation progressed. A future investigation could compare this visual approximation of the shear strain with an analytical method recently proposed by J. Pourtier et al. [36] that assumes simple shear as a unique deformation mode of the UD-NCF subjected to bias-extension loading. However, it should be noted that using a simple shear approximation may underestimate the shear strain developed in the material. The overall deformation, deformation features and shear strain that appeared in specimens texturized using the oil paint method closely resembled those of a bare fabric specimens.

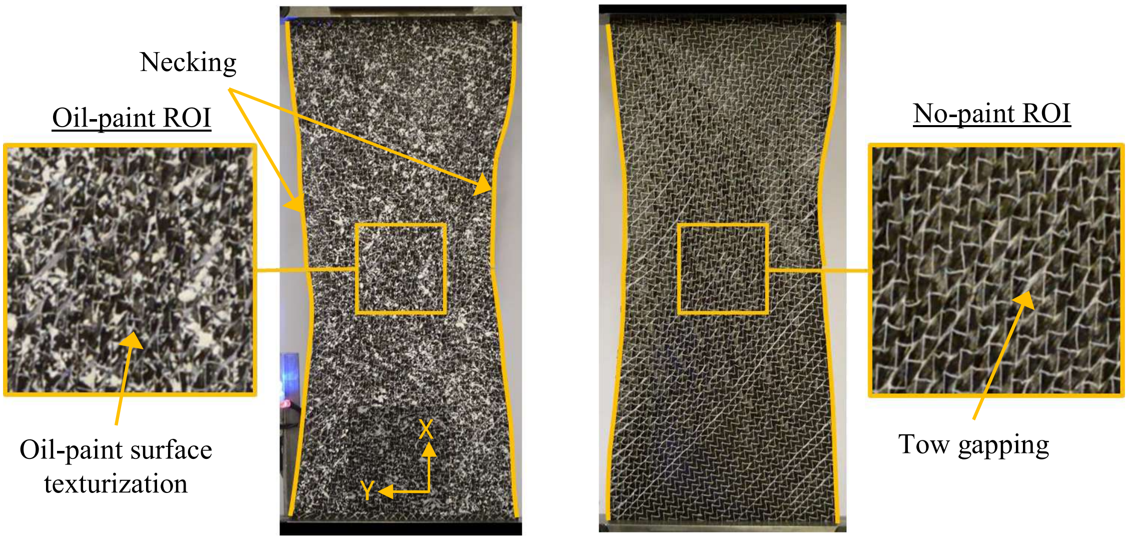

(a) **(b)**

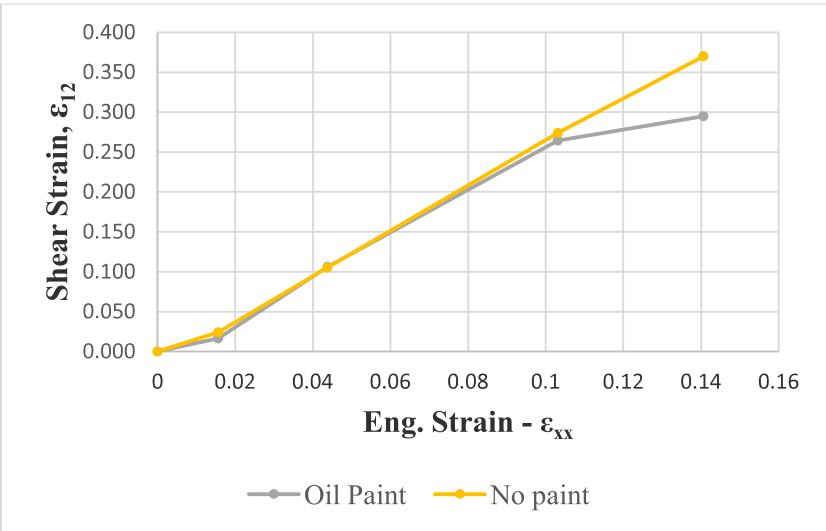

(c)

Fig. 15. Deformation after 33 mm of applied axial displacement during 45° off-axis extension test for (a) oil-paint texturized specimen and (b) bare fabric specimen. (c) Measurement of shear strain in the region of interest (ROI), with respect to the material coordinate system, of the oil painted and bare fabric specimens for the same off-axis extension tests.

6. Conclusions

The results of an investigation on the experimental techniques required to accurately capture the shear response of a carbon fiber (CF) unidirectional non-crimp fabric (UD-

NCF) subjected to biased uniaxial extension loading were presented. Three different surface texturization methods were employed on the UD-NCF material to facilitate optical strain measurements using digital image correlation (DIC). Also, a clamping design was proposed to prevent damage to the fabric while avoiding skewed test results during 45° off-axis testing and transverse uniaxial tensile testing. The ability to capture strains during displacement-controlled extension tests permitted the study of the interaction between shear and tension deformation modes. It was found that although shear was the prevalent deformation mode during the 45° off-axis test, compression and tensile strains are also evident parallel and perpendicular to the CF filaments.

The investigation of different surface texturization methods revealed that the use of conventional spray paint and latex-based paint were not adequate for surface texturization of CF UD-NCFs. A mixture of oil paint with 6% ml/ml mineral spirits concentration yielded the highest quality surface treatment for the DIC algorithm to accurately measure surface strains, while at the same time minimizing the mechanical reinforcing effect the paint had on the fabric. While the spray and latex paints increased the magnitude of force response of the fabric by more than 3 and 1.8 times respectively compared to bare fabric, the oil-paint treatment only slightly increased the fabric load response. More importantly, using oil-paint for surface texturization was an effective method to capture the distinctive interactions between shear and tensile deformation modes and accurately capture the load response of the fabric.

Additionally, a comparison of the overall deformation of a bare fabric specimen with a specimen texturized using the oil-based paint indicated that while surface texturization may slightly affect the load response, it did not have an effect on the deformation morphology of the fabric. Although additional experimental work should be conducted to verify the utility of this method for different fabric deformation conditions, the study provided a practical solution to one of the main challenges related to characterizing the deformation behavior of unbalanced UD-NCFs, which is a major contribution. Furthermore, the developed test protocol and the captured fabric deformation response are important aspects for accurately characterizing unbalanced UD-NCFs and for calibrating corresponding fabric constitutive models that are required to simulate draping for liquid moulding processes used to fabricate fiber-reinforced plastic components.

Acknowledgements

The authors thank the Natural Sciences and Engineering Research Council of Canada (NSERC) for supporting this study through funding grant CRDPJ-507776-16, as well as sponsors Honda R&D Americas, Hexion Inc., Zoltek Corp. and LAVAL International.

References

[1] Margossian A, Bel S, Balvers JM, Leutz D, Freitas R, Hinterhoelzl R. Finite element forming simulation of locally stitched non-crimp fabrics. Compos Part A Appl Sci Manuf 2014;61:152–62. doi:10.1016/J.COMPOSITESA.2014.02.020.

[2] Jauffrès D, Sherwood JA, Morris CD, Chen J. Discrete mesoscopic modeling for the simulation of woven-fabric reinforcement forming. Int J Mater Form 2010;3:1205–16. doi:10.1007/s12289-009-0646-y.

[3] Swentek I, Beck B, Ugresic V, Potyra T, Henning F. Impact of HP-RTM Process Parameters on Mechanical Properties Using Epoxy and Polyurethane. Compos Adv Mater Expo. Arlington, Oct. 26, 2015:1953–64.

[4] Haanappel S. Forming of UD fibre reinforced thermoplastics. PhD Thesis. University of Twente, 2013. doi:10.3990/1.9789036535014.

[5] Schirmaier FJ, Dörr D, Henning F, Kärger L. A macroscopic approach to simulate the forming behaviour of stitched unidirectional non-crimp fabrics (UD-NCF). Compos Part A Appl Sci Manuf 2017;102:322–35. doi:10.1016/j.compositesa.2017.08.009.

[6] Chen S, McGregor OPL, Harper LT, Endruweit A, Warrior NA. Defect formation during preforming of a bi-axial non-crimp fabric with a pillar stitch pattern. Compos Part A Appl Sci Manuf 2016;91:156–67. doi:10.1016/J.COMPOSITESA.2016.09.016.

[7] Boisse P, Hamila N, Madeo A. Modelling the development of defects during composite reinforcements and prepreg forming. Philos Trans R Soc A Math Phys Eng Sci 2016;374. doi:10.1098/rsta.2015.0269.

[8] Harrison P, Clifford MJ, Long AC. Shear characterisation of viscous woven textile composites: a comparison between picture frame and bias extension experiments. Compos Sci Technol 2004;64:1453–65. doi:10.1016/J.COMPSCITECH.2003.10.015.

[9] Lomov S V, Boisse P, Deluycker E, Morestin F, Vanclooster K, Vandepitte D, Verpoest I, Willems, A. Full-field strain measurements in textile deformability

studies. Compos Part A Appl Sci Manuf 2008;39:1232–44. doi:10.1016/j.compositesa.2007.09.014.

[10] Schirmaier FJ, Weidenmann KA, Kärger L, Henning F. Characterisation of the draping behaviour of unidirectional non-crimp fabrics (UD-NCF). Compos Part A Appl Sci Manuf 2016;80:28–38. doi:10.1016/J.COMPOSITESA.2015.10.004.

[11] Cao J, Akkerman R, Boisse P, Chen J, Cheng HS, de Graaf EF, Gorczyca JL, Harrison P, Hivet G, Launay J, Lee W, Liu L, Lomov SV, Long A, de Luycker E, Morestin F, Padvoiskis J, Peng XQ, Sherwood J, Stoilova Tz, Tao XM, Verpoest I, Willems A, Wiggers J, Yu TX, Zhu B. Characterization of mechanical behavior of woven fabrics: Experimental methods and benchmark results. Compos Part A Appl Sci Manuf 2008;39:1037–53. doi:10.1016/j.compositesa.2008.02.016.

[12] Ghazimoradi M, Naouar N, Carvelli V, Boisse P. Numerical modelling of the mechanical behaviour of tetraxial technical textiles. J Mater Sci 2019;54:3632–47. doi:10.1007/s10853-018-3084-8.

[13] Ghazimoradi M, Carvelli V, Naouar N, Boisse P. Experimental measurements and numerical modelling of the mechanical behaviour of a glass plain weave composite reinforcement. Reinf Plast Compos 2019;39:45-59. doi:10.1177/0731684419868846.

[14] Yu W-R, Harrison P, Long A. Finite element forming simulation for non-crimp fabrics using a non-orthogonal constitutive equation. Compos Part A Appl Sci Manuf 2005;36:1079–93. doi:10.1016/J.COMPOSITESA.2005.01.007.

[15] Boisse P. Advances in composites manufacturing and process design. Cambridge: Woodhead Publishing; 2015. doi:10.1016/C2014-0-02644-5.

[16] Bel S, Boisse P, Dumont F. Analyses of the Deformation Mechanisms of Non-Crimp Fabric Composite Reinforcements during Preforming. Appl Compos Mater 2012:513–28. doi:10.1007/s10443-011-9207-x.

[17] Mouritz AP. Introduction to aerospace materials. 1st ed. Cambridge: Woodhead Publishing; 2012. doi:10.1533/9780857095152.

[18] Laurenzi S, Marchetti M. Advanced Composite Materials by Resin Transfer Molding for Aerospace Applications. In: Hu N, editor. Compos. Their Prop. 1st ed., Rijeka: Intech; 2012, p. 197–226. doi:10.5772/48172.

[19] Boisse P, Hamila N, Guzman-Maldonado E, Madeo A, Hivet G, dell'Isola F. The bias-extension test for the analysis of in-plane shear properties of textile composite reinforcements and prepregs: a review. Int J Mater Form 2017;10:473–92. doi:10.1007/s12289-016-1294-7.

[20] Senner T, Kreissl S, Merklein M, Meinhardt M, Lipp A, Merklein M. Bending of unidirectional non-crimp-fabrics: experimental characterization, constitutive modeling and application in finite element simulation. Prod Eng 2015;9:1–10. doi:10.1007/s11740-014-0568-5.

[21] Bibo GA, Hogg PJ, Kemp M. Mechanical characterisation of glass- and carbon-

fibre-reinforced composites made with non-crimp fabrics. Compos Sci Technol 1997;57:1221–41. doi:10.1016/s0266-3538(97)00053-5.

[22] Arnold SE, Sutcliffe MPF, Oram WLA. Experimental measurement of wrinkle formation during draping of non-crimp fabric. Compos Part A Appl Sci Manuf 2016;82:159–69. doi:10.1016/J.COMPOSITESA.2015.12.011.

[23] Lomov S V., Truong Chi T, Verpoest I. Mechanical properties of non-crimp fabric (NCF) based composites: stiffness and strength. In: Lomov S V., editor. Non-Crimp Fabr. Compos. Manuf. Prop. Appl. 1st ed., Cambridge: Woodhead Publishing Limited; 2011, p. 1–523. doi:10.1533/9780857092533.

[24] Schneider M. Automated analysis of defects in non-crimp fabrics for composites. In: Lomov S V., editor. Non-Crimp Fabr. Compos. 1st ed., Cambridge: Woodhead Publishing Limited; 2011, p. 103–14. doi:10.1533/9780857092533.4.461.

[25] Rashidi A, Milani AS. A multi-step biaxial bias extension test for wrinkling/de-wrinkling characterization of woven fabrics: Towards optimum forming design guidelines. Mater Des 2018;146:273–85. doi:10.1016/J.MATDES.2018.02.075.

[26] Ghazimoradi M, Carvelli V, Marchesi MC, Frassine R. Mechanical characterization of tetraxial textiles. J Ind Text 2018;48:3–24. doi:10.1177/1528083717721920.

[27] Hosseini A, Kashani MH, Sassani F, Milani AS, Ko F. A Mesoscopic Analytical Model to Predict the Onset of Wrinkling in Plain Woven Preforms under Bias Extension Shear Deformation. Materials (Basel) 2017;10:1184. doi:10.3390/MA10101184.

[28] Hosseini A, Kashani MH, Sassani F, Milani AS, Ko FK. Identifying the distinct shear wrinkling behavior of woven composite preforms under bias extension and picture frame tests. Compos Struct 2018;185:764–73. doi:10.1016/j.compstruct.2017.11.033.

[29] King MJ, Jearanaisilawong P, Socrate S. A continuum constitutive model for the mechanical behavior of woven fabrics. Int J Solids Struct 2005;42:3867–96. doi:10.1016/J.IJSOLSTR.2004.10.030.

[30] Xiao S, Wang P, Soulat D, Legrand X, Gao H. Studies of in-plane shear behaviour of braided composite reinforcements. AIP Conf Proceedings. London, April 23, 2018. doi:10.1063/1.5034840.

[31] Xiao S, Wang P, Soulat D, Minet J, Zemni L, Gao H. Analysis of the in-plane shear behaviour of non-orthogonally textile reinforcements: Application to braided fabrics. Compos Part B Eng 2018;153:159–66. doi:10.1016/j.compositesb.2018.07.040.

[32] Senner T, Kreissl S, Merklein M, Meinhardt J, Lipp A, Kreissl S. A modular modeling approach for describing the in-plane forming behavior of unidirectional non-crimp-fabrics. Prod Eng Res Devel 2014;8:635–43. doi:10.1007/s11740-014-0561-z.

[33] Kovalev AE, Dening K, Persson BNJ, Gorb SN. Surface topography and contact

mechanics of dry and wet human skin. Beilstein J Nanotechnol 2014;5:1341–8. doi:10.3762/bjnano.5.147.

[34] Tekieli M, De Santis S, de Felice G, Kwiecień A, Roscini F. Application of Digital Image Correlation to composite reinforcements testing. Compos Struct 2017;160:670–88. doi:10.1016/J.COMPSTRUCT.2016.10.096.

[35] Harrison P, Taylor E, Alsayednoor J. Improving the accuracy of the uniaxial bias extension test on engineering fabrics using a simple wrinkle mitigation technique. Compos Part A Appl Sci Manuf 2018;108:53–61. doi:10.1016/j.compositesa.2018.02.025.

[36] Pourtier J, Duchamp B, Kowalski M, Wang P, Legrand X, Soulat D. Two-way approach for deformation analysis of non-crimp fabrics in uniaxial bias extension tests based on pure and simple shear assumption. Int J Mater Form 2019;12:995–1008. doi:10.1007/s12289-019-01481-8.

[37] Correlated Solutions. Vic-2D V6 Manual. 2009.

[38] Schreier H, Orteu J-J, Sutton MA. Image Correlation for Shape, Motion and Deformation Measurements. Boston, MA: Springer US; 2009. doi:10.1007/978-0-387-78747-3.

[39] Li J, Zeng D, Zhu X, Xu W, Zhang B, Yang L. Property and Fiber Orientation Determination for Carbon Fiber Composite. SAE Tech Pap 2018;2018-April:1–7. doi:10.4271/2018-01-1216.

[40] He T, Liu L, Makeev A, Shonkwiler B. Characterization of stress–strain behavior of composites using digital image correlation and finite element analysis. Compos Struct 2016;140:84–93. doi:10.1016/J.COMPSTRUCT.2015.12.018.